Figure 1.

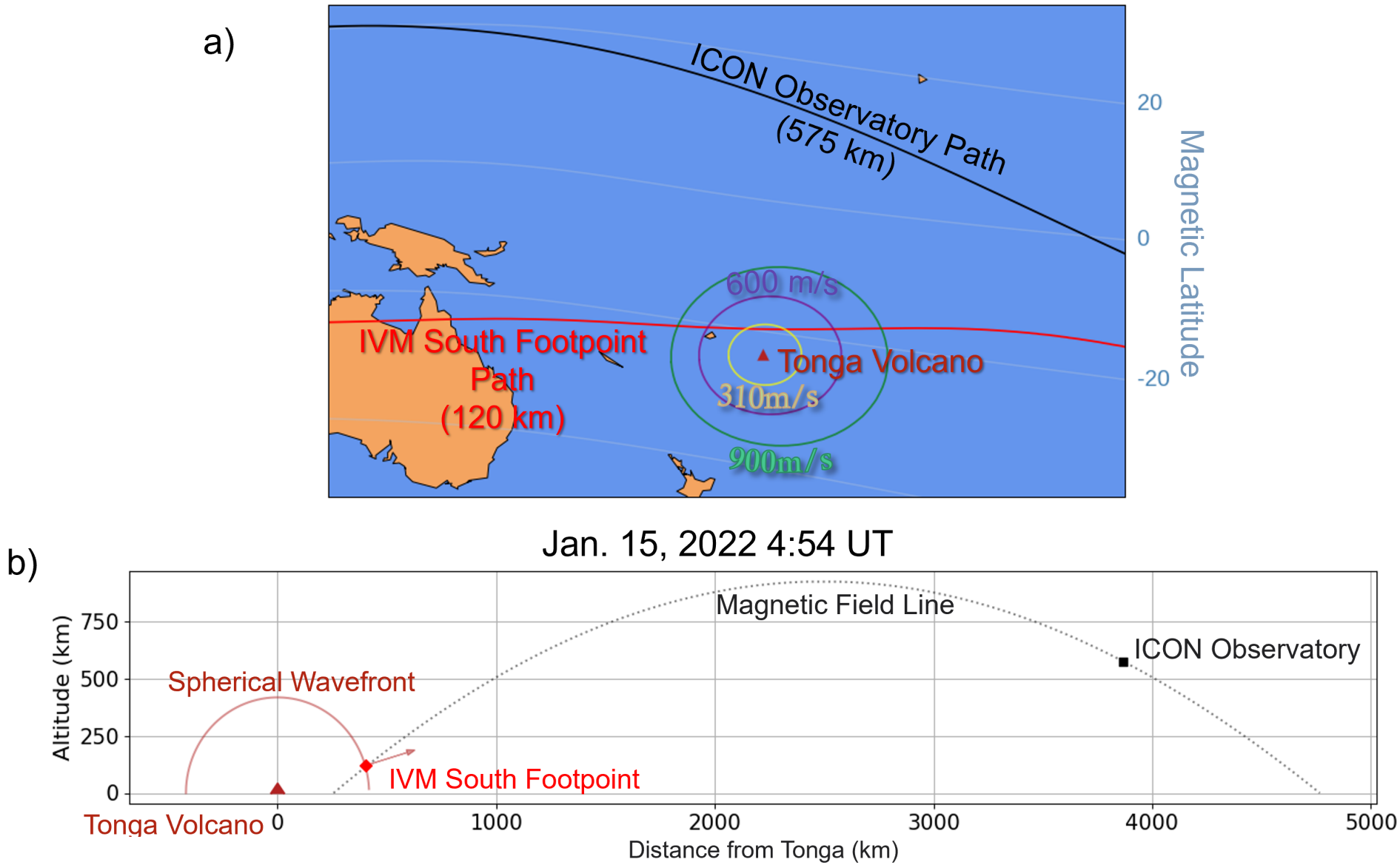
a)
ICON Observatory Path
(575 km)
IVM South Footpoint
Path
(120 km)
600 m/s
310m/s
900m/s
Tonga Volcano
20
0
-20
Magnetic Latitude
b)
Jan. 15, 2022 4:54 UT
Magnetic Field Line
ICON Observatory
Spherical Wavefront
IVM South Footpoint
Tonga Volcano
Altitude (km)
750
500
250
0
0
1000
2000
3000
4000
5000
Distance from Tonga (km)

Figure 2.

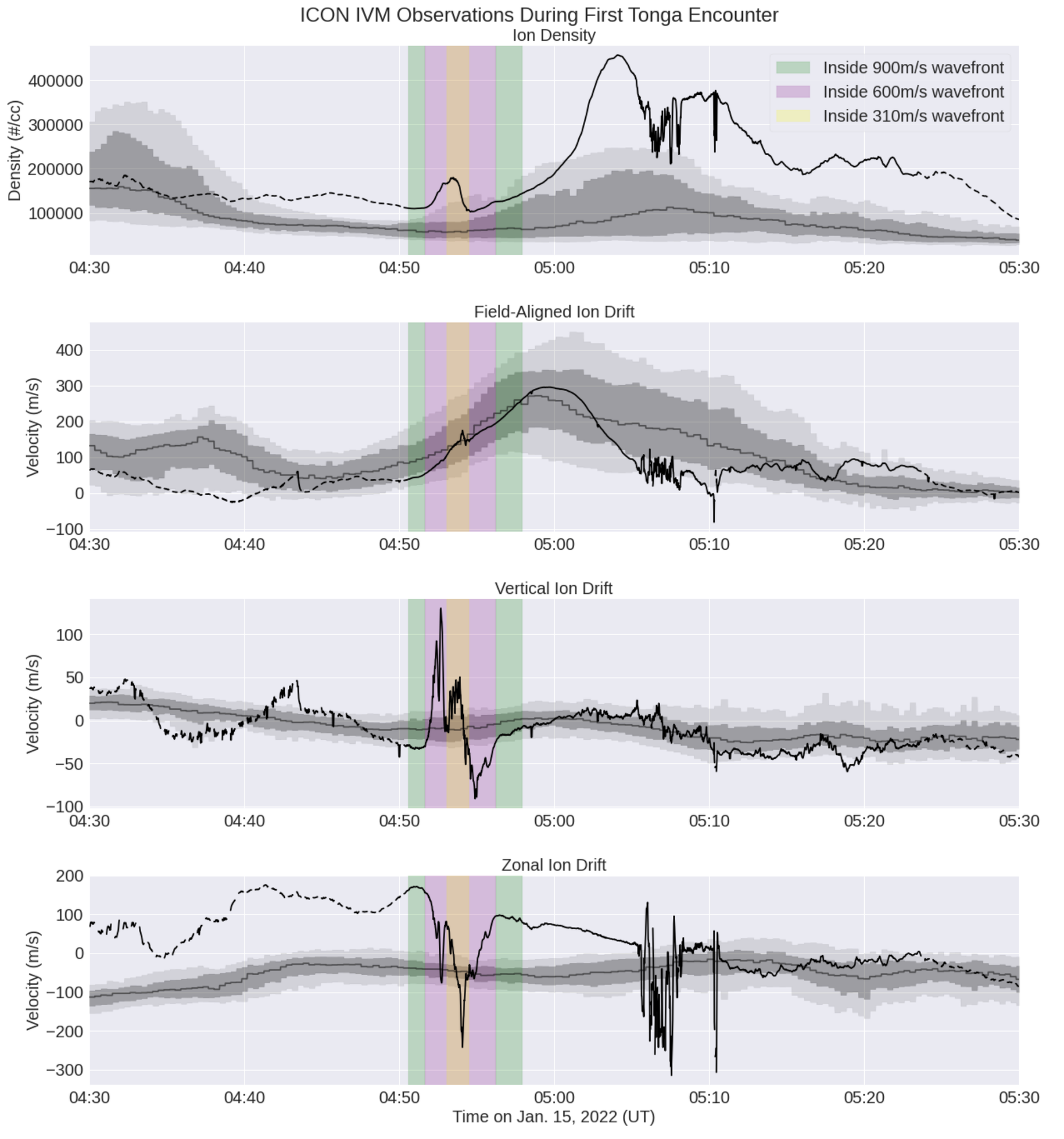
ICON IVM Observations During First Tonga Encounter
Ion Density
Density (#/cc)
400000
300000
200000
100000
Inside 900m/s wavefront
Inside 600m/s wavefront
Inside 310m/s wavefront
04:30
04:40
04:50
05:00
05:10
05:20
05:30
Field-Aligned Ion Drift
Velocity (m/s)
400
300
200
100
0
−100
Vertical Ion Drift
Velocity (m/s)
100
50
0
−50
−100
Zonal Ion Drift
Velocity (m/s)
200
100
0
−100
−200
−300
Time on Jan. 15, 2022 (UT)

Figure 3.

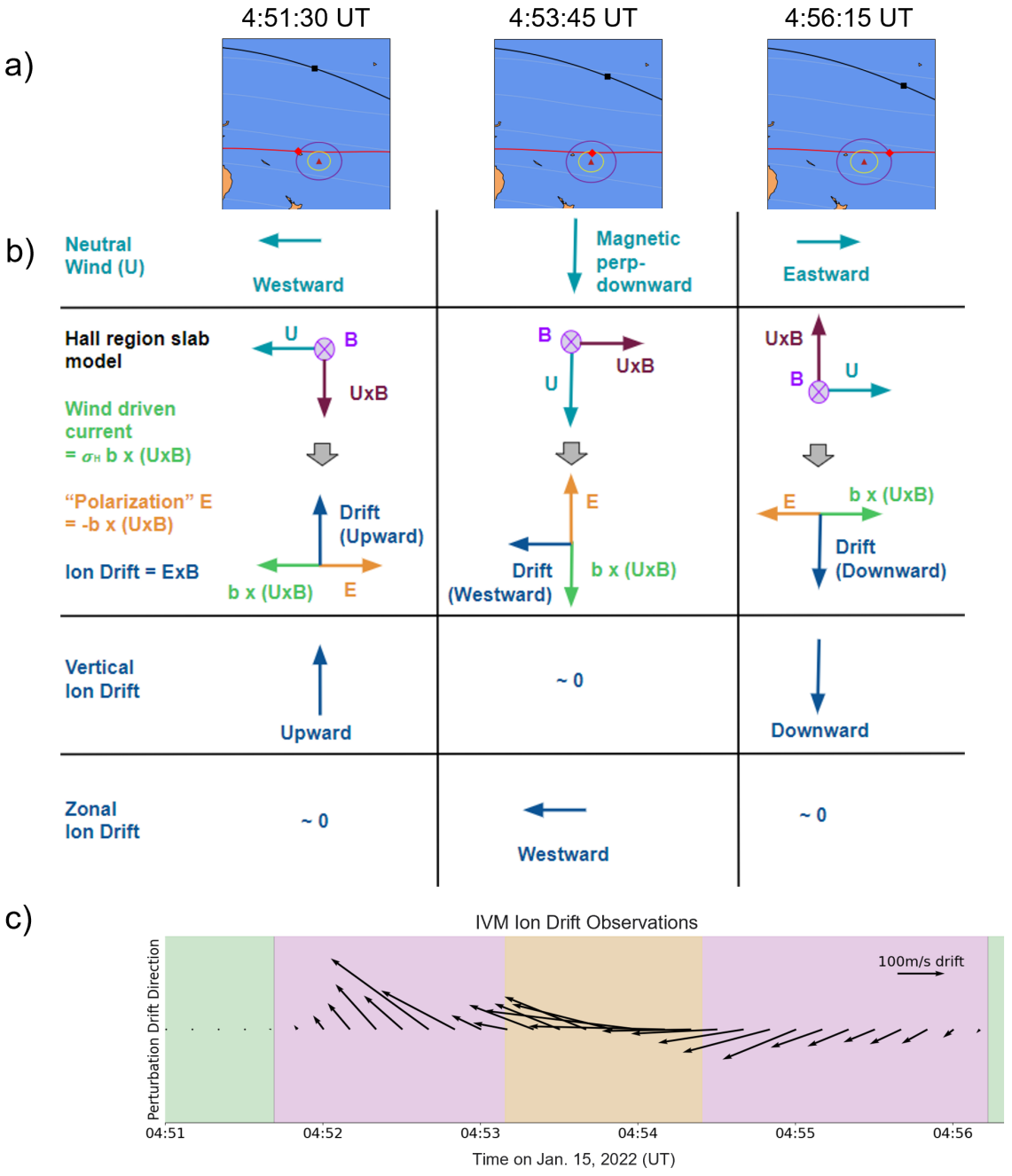
a)
4:51:30 UT
4:53:45 UT
4:56:15 UT
b)
Neutral Wind (U)
Westward
Magnetic perp-downward
Eastward
Hall region slab model
Wind driven current
= σH b x (UxB)
"Polarization" E
= -b x (UxB)
Ion Drift = ExB
U
B
UxB
Drift (Upward)
b x (UxB)
E
Drift (Westward)
Vertical Ion Drift
Upward
~ 0
Downward
Zonal Ion Drift
~ 0
Westward
~ 0
c)
IVM Ion Drift Observations
100m/s drift
Perturbation Drift Direction
04:51
04:52
04:53
04:54
04:55
04:56
Time on Jan. 15, 2022 (UT)

Rapid Volcanic Modification of the E-Region Dynamo: ICON's First Glimpse of the Tonga Eruption

L. Claire Gasque[1], Yen-Jung Wu[1], Brian J. Harding[1], Thomas J. Immel[1], Colin C. Triplett[1]

[1]University of California, Berkeley, Space Sciences Lab

Key Points:

- Extreme zonal and vertical ion drifts are observed ∼4000km away from Tonga less than an hour after the eruption, before any atmospheric wave arrived.
- The ion drifts are driven by volcanically forced polarization electric fields transmitted along Earth's magnetic field via Alfvén waves.
- The drift signature is consistent with the dynamo effect of an expanding atmospheric wave with a >200m/s amplitude.

Corresponding author: L. Claire Gasque, lcgasque@berkeley.edu

Abstract

The 15 Jan 2022 Hunga Tonga-Hunga Ha'apai volcano eruption drove global atmospheric waves that propagated into space and impacted the ionosphere. Here we show immediate large-scale electrodynamic effects of the eruption using observations from NASA's Ionospheric Connection Explorer. We report extreme zonal and vertical $\vec{E}\times\vec{B}$ ion drifts thousands of kilometers away from Tonga within an hour of the eruption, before the arrival of any atmospheric wave. The measured drifts were magnetically connected to the ionospheric E-region just 400km from Tonga, suggesting that the expanding wavefront created strong electric potentials which were transmitted along Earth's magnetic field. A simple theoretical model suggests that the observed drifts are consistent with an expanding wave with a large (>200 m/s) neutral wind amplitude. These observations are the first direct detection in space of the immediate electrodynamic effects of a volcanic eruption and will help constrain future models of impulsive lower atmospheric events.

Plain Language Summary

The Hunga Tonga-Hunga Ha'apai volcano eruption on 15 Jan 2022 sent seismic waves rippling through the Earth, launched tsunamis across the Pacific, and drove waves globally through the atmosphere. The atmospheric waves travelled into space, where they impacted the ionosphere, which extends from ∼80 to 1,000km above Earth's surface and is composed of ionized gas. Using observations from NASA's Ionospheric Connection Explorer, we show that the eruption dramatically modified charged particle motion in the ionosphere thousands of kilometers away from Tonga well before any atmospheric waves arrived. These changes are likely driven by strong electric fields generated near the volcano and transmitted along the Earth's magnetic field. A simple model suggests that the electric fields are generated by a fast neutral wind wavefront expanding away from the volcano. These observations are the first to measure the immediate ionospheric electrodynamic effects of a volcanic eruption, and will help calibrate models of the event, improving our understanding of how energy moves between the lower atmosphere and space.

1 Introduction

When it erupted on 15 Jan 2022, the submarine Hunga Tonga-Hunga Ha'apai volcano (subsequently called 'Tonga') released an immense amount of energy, with estimates ranging from 4 to 200 Megatons of TNT equivalent (Garvin, 2022; Astafyeva et al., 2022; Kulichkov et al., 2022; Vergoz et al., 2022). These energies are comparable to the energy released by the largest nuclear bombs, and rank the Tonga volcanic eruption as the strongest in the last 30 years (Duncombe, 2022). After the eruption, energy propagated outward via seismic waves traveling through the Earth (Poli & Shapiro, 2022), tsunamis moving across the ocean (Carvajal et al., 2022), and various acoustic and gravity wave modes propagating in the atmosphere, which were subsequently able to reach space and affect the ionosphere (Wright et al., 2022). Here, we will investigate the eruption's immediate ionospheric effect, examining how atmospheric waves emanating from the eruption rapidly modified the ionospheric dynamo, dramatically changing plasma behavior thousands of kilometers away.

The United States Geological Survey (USGS) used seismic data to estimate that the main volcanic blast occurred at 4:14:45 UT on 15 Jan 2022 (USGS, 2022). However, it took additional time for the effects of the blast to set up an atmospheric disturbance. The eruption vaporized the surrounding seawater, lofting more than 100 million tons of water vapor tens of kilometers into the stratosphere (Millan et al., 2022). There, the vapor again condensed and released its latent heat, transferring energy into the atmosphere and generating outward propagating waves (Wright et al., 2022). Maletckii and Astafyeva (2022) estimated that it would take approximately 11 minutes for energy to propagate

vertically from the volcano to the ionosphere assuming acoustic speeds. By backpropagating the observed pressure waves, Wright et al. (2022) found an atmospheric origin time of 4:28±2 UT, which we adopt for our analysis.

Once the waves were generated in the atmosphere, wave signatures were observed propagating horizontally around the globe. The most persistent of these had properties consistent with a Lamb wave, a non-dispersive pressure wave which propagated globally at speeds estimated between 300 and 390m/s (with most estimates around 310m/s), and whose signature was clearly distinguishable in total electron content (TEC) data taken by the Global Navigation Satellite System (GNSS) (Amores et al., 2022; Lin et al., 2022; Kataoka et al., 2022; Zhang et al., 2022; Kulichkov et al., 2022; Wright et al., 2022; Aa et al., 2022; Otsuka, 2022; Hong et al., 2022). Zhang et al. (2022) detected a TEC signature consistent with a propagating Lamb wave up to 100 hours after the eruption, after the wave had circled the globe at least three times.

Observations of previous volcanic eruptions, such as the 2015 Calbuco volcano, have also shown signatures of fast-moving wave modes (>500 m/s), which are mainly confined to within a few thousand kilometers of the source (Shults et al., 2016). For the Tonga eruption, close to the eruption site, TEC observations reported by Zhang et al. (2022) showed an initial supersonic infrasound wave traveling at ∼1 km/s for approximately 20 minutes, which, following Astafyeva (2019), they identified as consistent with a Rayleigh wave. Zhang et al. (2022) also deduced two shocks with initial radial propagation of ∼700 m/s which they observed slow to ∼450 m/s and which were confined to within 5000 km of the volcano. Similarly, Themens et al. (2022) reported a large scale TID radially propagating at 950 ± 170 m/s and a second TID propagating at 555 ± 45 m/s. Within 3000km, both of these waves reportedly slowed down to 550 ± 15 m/s and 390 ± 15 m/s, respectively. Astafyeva et al. (2022) used surface pressure data recorded only 64 km from Tonga, and found a likely propagation speed of ∼ 620 m/s for the ionospheric disturbance produced by the main eruption, which they posited to be due to a shock-acoustic wave mode due to its appearance as a sharp TEC increase. Additionally, Aa et al. (2022) reported observations of fast acoustic modes of 1050 m/s and 760 m/s from TEC data.

While many prior studies have investigated wave modes produced from volcanic eruptions, primarily using TEC data, few works have investigated the eruptions' impact on the ionospheric dynamo. TEC disturbances can result from a variety of mechanisms, including field-aligned drag, dynamo electric fields, and composition changes, but studies using TEC data alone are often unable to distinguish between these mechanisms. In one study which looked more closely at the dynamo mechanisms, Harding et al. (2022) investigated the Tonga eruption using data from the National Aeronautics and Space Administration's (NASA's) Ionospheric Connection Explorer (ICON) and the European Space Agency's (ESA's) Swarm satellites to observe extreme disruptions in the equatorial electrojet (EEJ) once the Lamb wave entered the dayside about 10 hours after the eruption. In particular, they reported that the EEJ disruption coincided with extreme (∼200 m/s) zonal winds in the dynamo region of the ionosphere (∼100-150 km). As noted by Harding et al. (2022), these winds are larger than 99.9% of winds observed for the entire ICON mission to date.

Here, we investigate the more immediate effects of the eruption on the E-region dynamo. Within an hour of the eruption, the ICON satellite sampled in situ ion drifts and densities on magnetic field lines with footpoints within 400km from Tonga. We report observations of extreme ion drifts consistent with extreme winds directed away from the eruption site, evidence of the volcano's influence on the ionospheric dynamo. In Section 2, we describe the data products and methods used to infer the volcanic effects. In Section 3, we present the observations and propose a theoretical model to interpret them. Finally, in Section 4 we conclude and suggest directions for future work.

2 Data and Methods

NASA's ICON mission was designed to explore energy and momentum transfer into the ionosphere from both solar and lower atmospheric sources (Immel et al., 2018). As a result, it is well-suited to study the effects of a volcanic eruption, a large impulsive lower atmospheric energy source. This study uses data from ICON's Ion Velocity Meter (IVM), which employs a Retarding Potential Analyzer (RPA) and Ion Drift Meter (IDM) to make in situ measurements of ion drifts and densities. For details on the design and principles behind the IVM, see Heelis et al. (2017).

The ICON observatory travels in a near-circular, 27° inclination orbit at roughly 575km altitude, with an orbital period of ∼97 minutes. The observatory passed within 4000km of the Tonga eruption site at around 4:54 UT, less than an hour after the eruption. Figure 1a depicts ICON's trajectory for its first orbit following the eruption. The observatory's path is shown in black. For reference, the locations of several nominal wavefronts with phase speeds of 310 m/s (yellow), 600 m/s (purple), and 900 m/s (green) are shown, roughly identifying the regions affected by waves reported by previous studies (see Section 1). We assume each of these waves propagates isotropically and at constant velocity from the eruption site with an origin time of 4:28 UT. The wavefronts are calculated at each longitude based on the time ICON's south magnetic footpoint (described further below) reaches that longitude, explaining why the wavefronts are slightly distorted. We neglect any potential influence from global wind patterns which may cause asymmetric propagation, despite some evidence that the waves did not propagate evenly in all directions and that some of the phase fronts slowed significantly in the near-field (Themens et al., 2022; Zhang et al., 2022; Astafyeva et al., 2022). As we are mainly using these regions as a tool to qualitatively reveal where it might be possible to observe the effects of the volcano, these considerations do not affect our interpretation.

While the path of the observatory itself does not pass through the region affected by the volcano during this initial pass, the IVM's south magnetic footpoint passes within 500km of Tonga. The south magnetic footpoint is identified in Figure 1b as the point in the ionospheric E-region (at 120 km) connected to the same magnetic field line as the observatory, which is calculated using quasi-dipole coordinates (Emmert et al., 2010). Although the IVM makes measurements in situ at the observatory, ion drifts are driven by electric fields which are rapidly transmitted along magnetic field lines via Alfvén waves. The electric fields are therefore the same at all points along a single magnetic field line, assuming the field lines are equipotentials (Heelis et al., 2017). Daytime electric fields are typically dominated by forcing in the E-region where the Hall and Pedersen conductivities are highest. Therefore, the ion drifts ICON measures during this pass are likely to be affected by the eruption.

To distinguish differences in the observed drifts from what would be expected at these solar local times (SLTs), we established a background climatology using ion drift data from 8 - 13 Jan, 2022, during which magnetic conditions were relatively quiet. We excluded data from 14 Jan 2022 (the day before the eruption) to avoid contamination from a moderate geomagnetic storm which occurred on that day. The climatology was performed by sorting the data on a 6-minute SLT grid and finding the median as well as the 90th, 75th, 25th, and 10th quantiles.

3 Results and Discussion

Figure 2 presents ICON IVM ion density and drift measurements for the first orbit following the Tonga eruption. The green, purple, and yellow highlighted regions correspond to the nominal wavefronts shown in Figure 1a, representing wavefronts traveling at 900 m/s, 600 m/s, and 310 m/s, respectively. The SLT climatology is shown in gray, with the dark gray line representing the median of the measurements, the dark gray re-

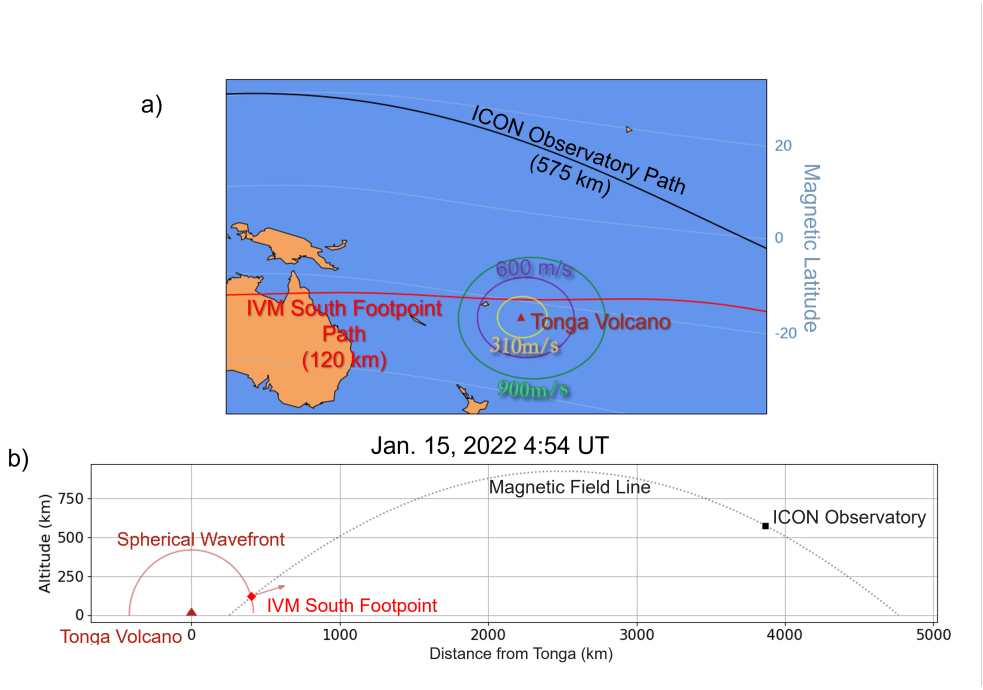

Figure 1. (a) ICON's geographic and south magnetic footpoint positions relative to the Tonga volcano. Also shown are wavefronts for disturbances traveling from the eruption site at 310 m/s (yellow), 600 m/s (purple) and 900 m/s (green). The wavefronts are assumed to propagate isotropically at constant velocity, and are shown at the moment that the IVM south footpoint is at the same longitude as the wavefront. (b) The magnetic field line connected to ICON at its closest approach to Tonga, showing the IVM south magnetic footpoint. A simple spherical wavefront model shows that when the IVM south magnetic footpoint is north of the volcano, the normal to it points mostly northward.

gion bounding the 25th to 75th quantiles, and the light gray region bounding the 10th to 90th quantiles. In particular, note the extreme vertical and zonal ion drifts observed within the region affected by the volcano, peaking at 6.9σ and 8.8σ respectively with respect to the quiet-time climatology. In addition, we observe a modest increase in the density, and little change in the field aligned drift during the same period.

The observations occur during the recovery phase of the 14 Jan geomagnetic storm. We argue that the observed extreme ion drifts are dominated by volcanic forcing, not geomagnetic influences. If present, storm-induced penetration electric fields could theoretically influence ion drifts, although the effects would be largely independent of longitude. The extreme variation in the vertical and zonal ion drifts ICON observes are confined to only the longitudes already under the influence of the disturbances propagating away from the volcano, suggesting they are directly related to the effects of the eruption. Furthermore, as Harding et al. (2022) showed, there is no evidence of large penetration electric fields due to the storm. One likely effect is a storm-related deviation of the zonal ion drifts from the climatology prior to and following the region affected by the volcano. This deviation in the background zonal drifts begins around 19UT on 14 Jan 2022, near the onset of the storm, and is also seen during previous and future orbits on this day (not shown). The feature beginning at around 6:05 UT is equatorial spread-F, which occurs shortly after the observatory crosses the solar terminator, and is unrelated to the eruption.

ICON first observes the volcanically-driven ion drifts at ∼4:51:40 UT, determined using the time of the abrupt change in slope in the vertical ion drift in Figure 2. Similarly, ICON no longer observed the volcanically-driven ion drift perturbation at 4:56:30 UT. Given the observatory's location >4000 km from Tonga, the wavefront would have had to propagate at 3000±250 m/s to reach the observatory at the observed time, which is far faster than any known ionospheric wave mode. In order to reach ICON's south magnetic footpoint in the same time, the wavefront would need to propagate at 600±50 m/s. This observation is in line with wavefront velocities inferred by Zhang et al. (2022), Themens et al. (2022), and Astafyeva et al. (2022). Therefore, the extreme vertical and zonal ion drifts are likely $\vec{E}\times\vec{B}$ ion drifts resulting from polarization electric fields (PEFs) caused by the ion drag established by the eruption's forcing of the neutral atmosphere. The PEFs are transmitted almost instantaneously along the magnetic field line to the observatory's location via Alfvén waves (Kikuchi & Araki, 1979). These observations are direct evidence that the electrodynamic effects of the volcano were rapidly transmitted to the conjugate hemisphere.

To investigate the origin of the observed ion drifts, we consider a simple theoretical model of how the neutral winds driven by the volcano might drive the ionospheric dynamo. As a simple model, we consider the eruption to drive a spherically expanding wavefront pushing a neutral wind away from Tonga, as depicted in Figure 1b. As the IVM footpoint transits the affected region (Figure 3a), we would therefore expect it to encounter first a primarily westward, then northward, then eastward wind.

In order to determine the PEFs and resulting $\vec{E}\times\vec{B}$ ion drifts generated by this wind model, we use a theoretical slab model of the ionosphere following Kelley (2009). In this model, currents in the Hall region (∼100-120 km altitude) drive the electric fields along the slab of the ionosphere surrounding a single magnetic field line. Hall currents flow in the $\hat{b}\times(\vec{U}\times\vec{B})$ direction, where $\hat{b}$ is a unit vector in the magnetic field direction, $\vec{U}$ is the neutral wind, and $\vec{B}$ is the magnetic field. The wind-driven current causes a separation of charges, which sets up an opposing PEF in the $-\hat{b}\times(\vec{U}\times\vec{B})$ direction. This, in turn, will cause an $\vec{E}\times\vec{B}$ ion drift in the $(-\hat{b}\times(\vec{U}\times\vec{B}))\times\vec{B}$ direction, which is the same as the $\hat{b}\times\vec{U}$ direction.

Figure 3b uses this theoretical model to predict the direction of the observed drifts given the neutral wind input. Adopting a coordinate system where the magnetic field

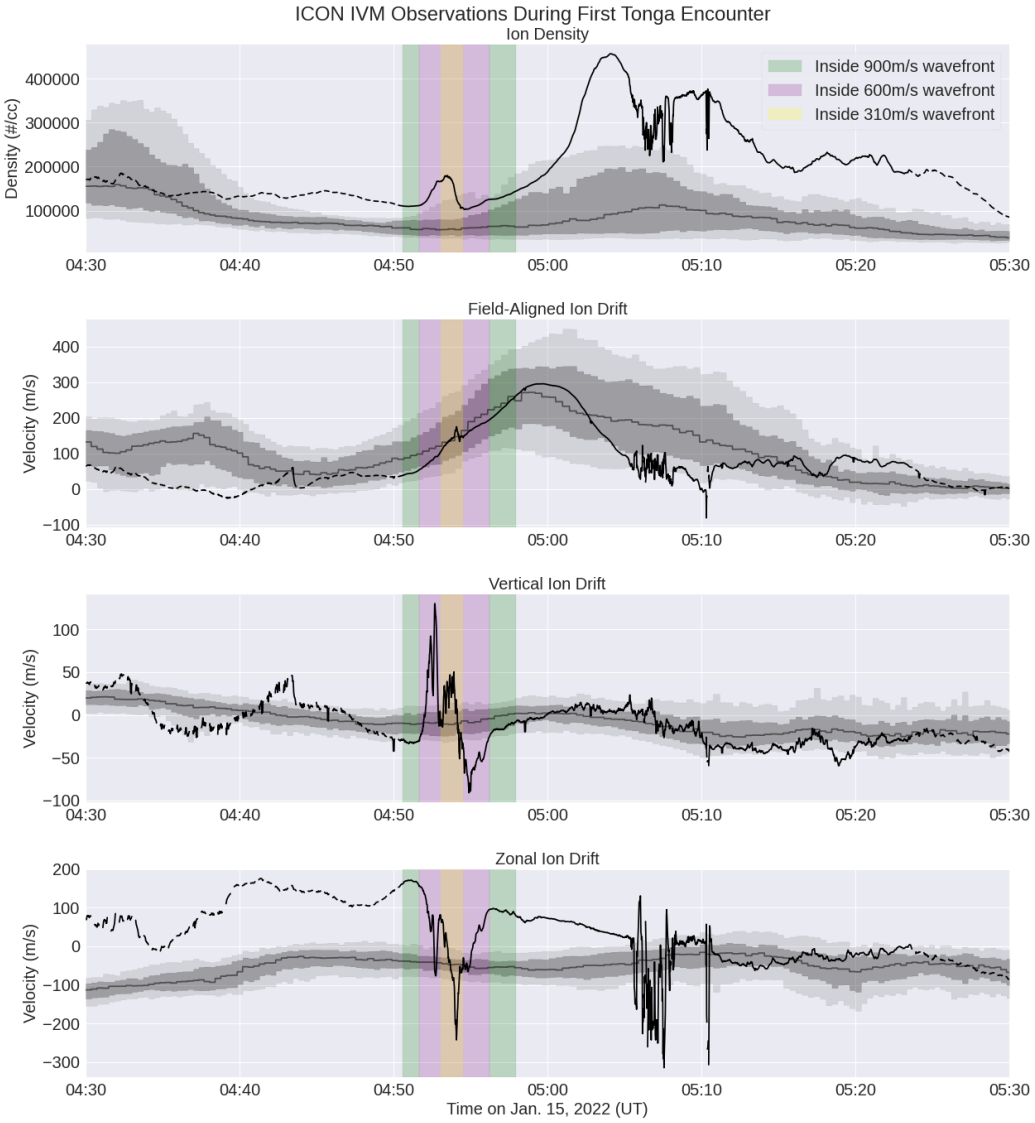

Figure 2. IVM ion density and drift measurements during ICON's orbit following the Tonga eruption. The data taken when the south footpoint was within nominal wavefronts moving at 900 m/s, 600 m/s, and 310 m/s are highlighted in green, purple, and yellow, respectively. The SLT climatologies are shown in gray, with light gray bounding the 10th to 90th quantiles, dark gray bounding the 25th to 75th quantiles, and the median shown as the darker gray line. Note the extreme vertical and zonal ion drifts in the region affected by the volcano.

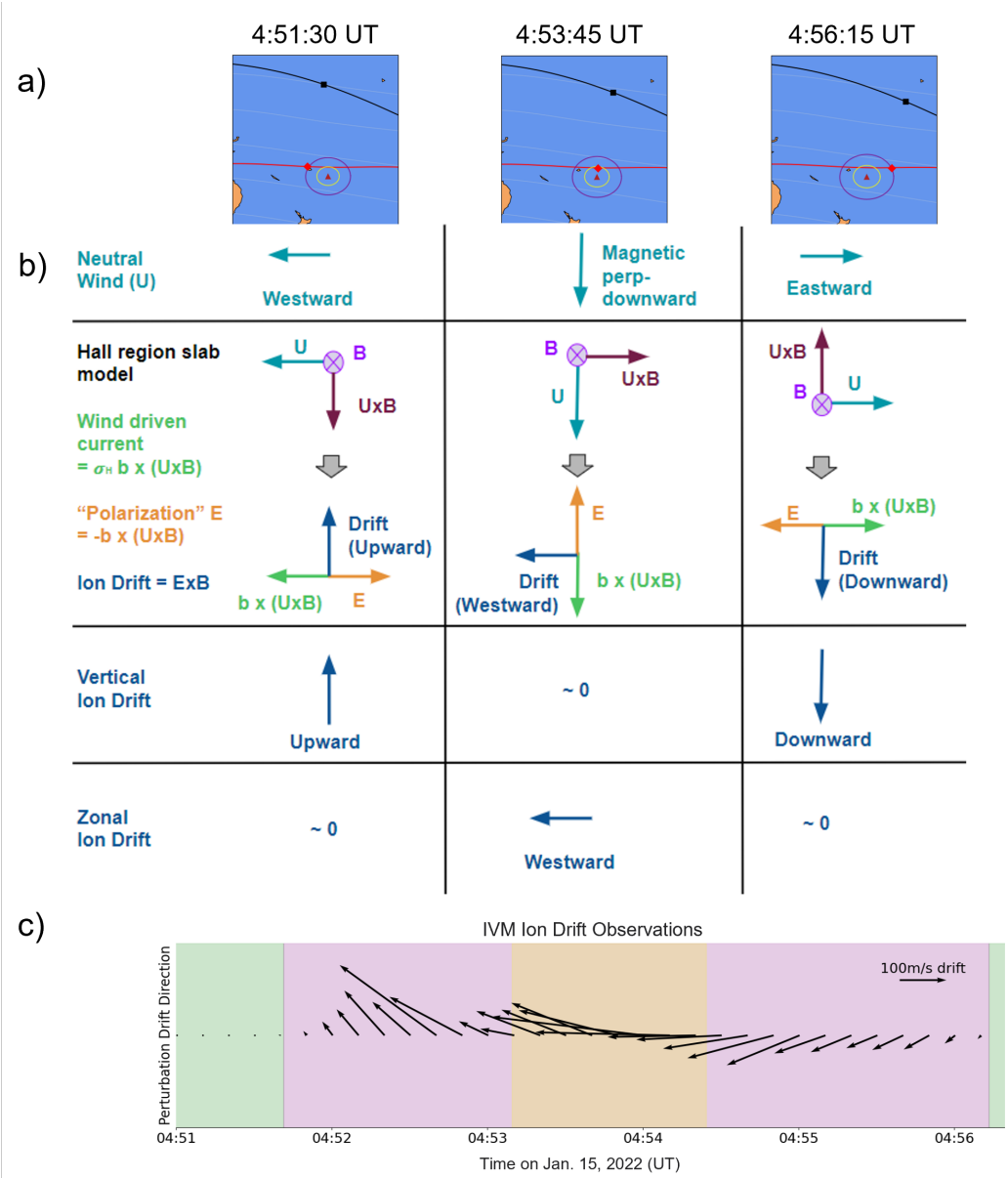

Figure 3. Predictions from a simplified slab model of Hall region currents driving the ionospheric dynamo (see text for details). (a) The locations of the ICON observatory and IVM south footpoint with respect to the expanding 600m/s (purple) and 310 m/s (yellow) wavefronts at times which correspond to the westward, northward, and eastward neutral winds. (b) A chart showing predicted ion drifts given the assumed neutral wind input. The top row shows the neutral wind input, the middle shows the determination of the ion drift direction from PEF established by the Hall region current. The bottom two rows show the theoretically predicted vertical and zonal ion drifts. (c) The IVM drift data with a linear trend removed aligned with the columns of the chart above. Upward pointing arrows represent upward perturbation drifts and rightward pointing arrows represent eastward perturbation drifts. These observations show good agreement with the theoretical results.

points into the page, the east and west point right and left, respectively, and the component of the northward neutral wind perpendicular to the magnetic field line will point down. Assuming the IVM south footpoint encounters first a westward, then northward, then eastward neutral wind, the Hall-region slab model predicts we will observe first upward, then westward, then downward ion drifts. Figure 3c shows perturbations in IVM ion drift observations from the background during the same time period. A linear trend between 4:51 and 4:57 UT (immediately before and after we observe the volcanogenic drift perturbations) has been subtracted from the drift data to better distinguish the perturbation due to the volcano from the background variation. The theoretical model succeeds at explaining the large-scale structure in the observed drifts; we first observe a predominantly upward, then westward, then downward ion drift, as predicted.

The theory does not perfectly match the observations, likely because of the model's simplicity. Even when the drifts are predominantly vertical, they still have a considerable westward component. This is partially due to the fact that, since the IVM south footpoint passes equator-ward of Tonga, there will be a northward wind component even when the neutral wind is predominantly zonal. Thus, we should expect to see a westward zonal drift component throughout the pass. The model also neglects Pedersen currents, which would add a component to the wind-driven current in the $\vec{U}\times\vec{B}$ direction, altering the direction of the PEF and resulting $\vec{E}\times\vec{B}$ ion drift. While both Hall and Pedersen region currents contribute to the $\vec{E}\times\vec{B}$ drifts in the evening at low latitudes (Maute et al., 2012), our model with the Hall currents alone reproduces the large scale ion drift features. A full theoretical treatment would necessarily include Pedersen currents as well as non-local effects.

This theoretical model also predicts that the magnitude of the ion drifts will be the same as the magnitude of the driving neutral wind. The IVM observed a maximum perturbation drift speed of 330 m/s, suggesting that the volcano drove neutral winds in the ionosphere at comparable speeds. While we do not have measurements of the neutral winds at the same times as these drift observations since the field-of-view of the neutral wind measurement is looking further north, Harding et al. (2022) reported Hall-region winds exceeding 200 m/s several hours following the Tonga eruption, suggesting that the inferred speeds are reasonable. The simplified model assumes perfect dynamo driving efficiency, which is unlikely given the simplifications above, as well as the influence of the northern footpoint winds. Thus, it is likely that the volcanogenic winds would need to be larger than 330 m/s to explain the observed drift perturbations.

4 Conclusion

In this work, we reported ICON IVM ion drift measurements for the first orbit following the 15 Jan 2022 Tonga volcanic eruption. Although the ICON observatory passed ∼4000 km away from the site of the eruption, it was magnetically connected to the ionospheric E-region just 400 km from Tonga, allowing the IVM to remotely sample the dynamo region close to Tonga within an hour of the main eruption.

We observed extreme vertical and zonal ion drifts, with maximum drift velocity perturbations exceeding 300 m/s. We find that the observed ion drifts appear too soon to be forced by a wave with a 310m/s group velocity. An effective propagation velocity of 600±50 m/s is needed to explain the arrival of the ion drift signature given the 4:28±0:02 origination time found by Wright et al. (2022). A simple theoretical model revealed that the changing direction of the drifts as ICON's IVM south magnetic footpoint transited the region affected by the volcano was largely consistent with the electrodynamic effects of a high amplitude (>300 m/s) neutral wind wavefront expanding away from the eruption site. These observations are also clear evidence of a conjugate effect: electric fields established by wind-driven currents in the vicinity of the volcano were transported to

the observatory's location via Alfvén waves, and arrived much sooner than any reported atmospheric waves.

Here, we focused only on ICON's IVM data from its first pass following the eruption. In addition to the IVM, ICON carries remote sensing instruments capable of measuring neutral winds, temperatures, and ion density profiles (Mende et al., 2017; Sirk et al., 2017; Englert et al., 2017; Stephan et al., 2017, 2018; Kamalabadi et al., 2018). During this orbit, the fields-of-view of ICON's remote sensing instruments were north of the observatory's path, outside of the region already influenced by the volcano, and so were unable to observe any volcanic effects. During later orbits, however, multiple ICON instruments can simultaneously observe the affected region. Although for this orbit we had to assume a neutral wind profile to predict the observed ion drift dynamics, future work will use observed neutral winds and drifts to investigate multiple aspects of the thermosphere/ionosphere effects of the eruption, applying methods described in Immel et al. (2021). Later orbits will likely be additionally complicated by a combination of dynamo forcing and direct drag acting on the ionosphere, as well as interactions between different direct and conjugate wavefronts.

The observations reported here are the first direct detection in space of the near-immediate dynamo effects of a volcanic eruption, and will prove iconic for constraining ionospheric models of this and other impulsive lower atmospheric events.

Acknowledgments

ICON is supported by NASA's Explorers Program through contracts NNG12FA45C and NNG12FA42I. ICON data are processed and available in the ICON Science Data Center at the University of California, Berkeley and are available at `https://icon.ssl.berkeley.edu/Data`

References

Aa, E., Zhang, S.-R., Erickson, P. J., Vierinen, J., Coster, A. J., Goncharenko, L. P., ... Rideout, W. (2022). Significant equatorial plasma bubbles and global ionospheric disturbances after the 2022 tonga volcano eruption. *Earth and Space Science Open Archive*, 17. Retrieved from `https://doi.org/10.1002/essoar.10510637.1` doi: 10.1002/essoar.10510637.1

Amores, A., Monserrat, S., Marcos, M., Argüeso, D., Villalonga, J., Jordà, G., & Gomis, D. (2022). Numerical simulation of atmospheric lamb waves generated by the 2022 hunga-tonga volcanic eruption. *Geophysical Research Letters*, e2022GL098240.

Astafyeva, E. (2019). Ionospheric detection of natural hazards. *Reviews of Geophysics*, *57*(4), 1265–1288.

Astafyeva, E., Maletckii, B., Mikesell, T. D., Munaibari, E., Ravanelli, M., Coïsson, P., ... Rolland, L. (2022). The 15 january 2022 hunga tonga eruption history as inferred from ionospheric observations. *Geophysical Research Letters*, *49*(10), e2022GL098827.

Carvajal, M., Sepúlveda, I., Gubler, A., & Garreaud, R. (2022). Worldwide signature of the 2022 tonga volcanic tsunami. *Geophysical Research Letters*, e2022GL098153.

Duncombe, J. (2022). The surprising reach of tonga's giant atmospheric waves. *Eos*, *103*.

Emmert, J., Richmond, A., & Drob, D. (2010). A computationally compact representation of magnetic-apex and quasi-dipole coordinates with smooth base vectors. *Journal of Geophysical Research: Space Physics*, *115*(A8).

Englert, C. R., Harlander, J. M., Brown, C. M., Marr, K. D., Miller, I. J., Stump, J. E., ... others (2017). Michelson interferometer for global high-resolution

thermospheric imaging (mighti): instrument design and calibration. *Space science reviews*, *212*(1), 553–584.

Garvin, J. (2022). *Dramatic changes at hunga tonga-hunga ha'apai* [Text.Article]. Retrieved 2022-07-19, from `https://earthobservatory.nasa.gov/images/149367/dramatic-changes-at-hunga-tonga-hunga-haapai` (Publisher: NASA Earth Observatory)

Harding, B. J., Wu, Y.-J. J., Alken, P., Yamazaki, Y., Triplett, C., Immel, T. J., ... Xiong, C. (2022). Impacts of the january 2022 tonga volcanic eruption on the ionospheric dynamo: Icon-mighti and swarm observations of extreme neutral winds and currents.

Heelis, R., Stoneback, R., Perdue, M., Depew, M., Morgan, W., Mankey, M., ... Holt, B. (2017). Ion velocity measurements for the ionospheric connections explorer. *Space science reviews*, *212*(1), 615–629.

Hong, J., Kil, H., Lee, W. K., Kwak, Y.-S., Choi, B.-K., & Paxton, L. J. (2022). Detection of different properties of ionospheric perturbations in the vicinity of the korean peninsula after the hunga-tonga volcanic eruption on 15 january 2022. *Geophysical Research Letters*, *49*(14), e2022GL099163.

Immel, T. J., England, S., Mende, S., Heelis, R., Englert, C., Edelstein, J., ... others (2018). The ionospheric connection explorer mission: mission goals and design. *Space Science Reviews*, *214*(1), 1–36.

Immel, T. J., Harding, B. J., Heelis, R. A., Maute, A., Forbes, J. M., England, S. L., ... others (2021). Regulation of ionospheric plasma velocities by thermospheric winds. *Nature geoscience*, *14*(12), 893–898.

Kamalabadi, F., Qin, J., Harding, B. J., Iliou, D., Makela, J. J., Meier, R., ... Immel, T. J. (2018). Inferring nighttime ionospheric parameters with the far ultraviolet imager onboard the ionospheric connection explorer. *Space science reviews*, *214*(4), 1–14.

Kataoka, R., Winn, S. D., & Touber, E. (2022). Meteotsunamis in japan associated with the tonga eruption in january 2022. *SOLA*.

Kelley, M. C. (2009). *The earth's ionosphere: plasma physics and electrodynamics*. Academic press.

Kikuchi, T., & Araki, T. (1979). Horizontal transmission of the polar electric field to the equator. *Journal of Atmospheric and Terrestrial Physics*, *41*(9), 927–936.

Kulichkov, S., Chunchuzov, I., Popov, O., Gorchakov, G., Mishenin, A., Perepelkin, V., ... others (2022). Acoustic-gravity lamb waves from the eruption of the hunga-tonga-hunga-hapai volcano, its energy release and impact on aerosol concentrations and tsunami. *Pure and Applied Geophysics*, 1–16.

Lin, J.-T., Rajesh, P. K., Lin, C. C., Chou, M.-Y., Liu, J.-Y., Yue, J., ... Kung, M.-M. (2022). Rapid conjugate appearance of the giant ionospheric lamb wave in the northern hemisphere after hunga-tonga volcano eruptions.

Maletckii, B., & Astafyeva, E. (2022). Near-real-time analysis of the ionospheric response to the 15 january 2022 hunga tonga-hunga ha'apai volcanic eruption.

Maute, A., Richmond, A., & Roble, R. (2012). Sources of low-latitude ionospheric e× b drifts and their variability. *Journal of Geophysical Research: Space Physics*, *117*(A6).

Mende, S., Frey, H., Rider, K., Chou, C., Harris, S., Siegmund, O., ... others (2017). The far ultra-violet imager on the icon mission. *Space Science Reviews*, *212*(1), 655–696.

Millan, L., Santee, M. L., Lambert, A., Livesey, N. J., Werner, F., Schwartz, M. J., ... others (2022). The hunga tonga-hunga ha'apai hydration of the stratosphere.

Otsuka, S. (2022). Visualizing lamb waves from a volcanic eruption using meteorological satellite himawari-8. *Geophysical Research Letters*, *49*(8), e2022GL098324.

Poli, P., & Shapiro, N. M. (2022). Rapid characterization of large volcanic eruptions:

measuring the impulse of the hunga tonga explosion from teleseismic waves.

Shults, K., Astafyeva, E., & Adourian, S. (2016). Ionospheric detection and localization of volcano eruptions on the example of the april 2015 calbuco events. *Journal of Geophysical Research: Space Physics*, *121*(10), 10–303.

Sirk, M. M., Korpela, E. J., Ishikawa, Y., Edelstein, J., Wishnow, E. H., Smith, C., ... others (2017). Design and performance of the icon euv spectrograph. *Space science reviews*, *212*(1), 631–643.

Stephan, A. W., Korpela, E. J., Sirk, M. M., England, S. L., & Immel, T. J. (2017). Daytime ionosphere retrieval algorithm for the ionospheric connection explorer (icon). *Space science reviews*, *212*(1), 645–654.

Stephan, A. W., Meier, R., England, S. L., Mende, S. B., Frey, H. U., & Immel, T. J. (2018). Daytime o/n2 retrieval algorithm for the ionospheric connection explorer (icon). *Space science reviews*, *214*(1), 1–17.

Themens, D. R., Watson, C., Žagar, N., Vasylkevych, S., Elvidge, S., McCaffrey, A., ... Jayachandran, P. (2022). Global propagation of ionospheric disturbances associated with the 2022 tonga volcanic eruption. *Geophysical Research Letters*, e2022GL098158.

USGS. (2022). *M 5.8 volcanic eruption - 68 km NNW of nuku'alofa, tonga.* Retrieved 2022-07-20, from `https://earthquake.usgs.gov/earthquakes/eventpage/pt22015050/origin/detail`

Vergoz, J., Hupe, P., Listowski, C., Le Pichon, A., Garcés, M., Marchetti, E., ... others (2022). Ims observations of infrasound and acoustic-gravity waves produced by the january 2022 volcanic eruption of hunga, tonga: A global analysis. *Earth and Planetary Science Letters*, *591*, 117639.

Wright, C. J., Hindley, N. P., Alexander, M. J., Barlow, M., Hoffmann, L., Mitchell, C. N., ... others (2022). Surface-to-space atmospheric waves from hunga tonga-hunga ha'apai eruption. *Nature*, 1–3.

Zhang, S.-R., Vierinen, J., Aa, E., Goncharenko, L., Erickson, P., Rideout, W., ... Spicher, A. (2022). 2022 tonga volcanic eruption induced global propagation of ionospheric disturbances via lamb waves.